Nuclear Science and Techniques (2023) 34:32
https://doi.org/10.1007/s41365-023-01176-5

Verification of neutron-induced fission product yields evaluated by a tensor decompsition model in transport-burnup simulations

Qu-Fei Song[1,2] · Long Zhu[2] · Hui Guo[1] · Jun Su[2]

Received: 28 September 2022 / Revised: 9 December 2022 / Accepted: 12 December 2022 / Published online: 3 March 2023

Abstract

Neutron-induced fission is an important research object in basic science. Moreover, its product yield data are an indispensable nuclear data basis in nuclear engineering and technology. The fission yield tensor decomposition (FYTD) model has been developed and used to evaluate the independent fission product yield. In general, fission yield data are verified by the direct comparison of experimental and evaluated data. However, such direct comparison cannot reflect the impact of the evaluated data on application scenarios, such as reactor transport-burnup simulation. Therefore, this study applies the evaluated fission yield data in transport-burnup simulation to verify their accuracy and possibility of application. Herein, the evaluated yield data of ^{235}U and ^{239}Pu are applied in the transport-burnup simulation of a pressurized water reactor (PWR) and sodium-cooled fast reactor (SFR) for verification. During the reactor operation stage, the errors in pin-cell reactivity caused by the evaluated fission yield do not exceed 500 and 200 pcm for the PWR and SFR, respectively. The errors in decay heat and ^{135}Xe and ^{149}Sm concentrations during the short-term shutdown of the PWR are all less than 1%; the errors in decay heat and activity of the spent fuel of the PWR and SFR during the temporary storage stage are all less than 2%. For the PWR, the errors in important nuclide concentrations in spent fuel, such as ^{90}Sr, ^{137}Cs, ^{85}Kr, and ^{99}Tc, are all less than 6%, and a larger error of 37% is observed on ^{129}I. For the SFR, the concentration errors of ten important nuclides in spent fuel are all less than 16%. A comparison of various aspects reveals that the transport-burnup simulation results using the FYTD model evaluation have little difference compared with the reference results using ENDF/B-VIII.0 data. This proves that the evaluation of the FYTD model may have application value in reactor physical analysis.

Keywords Fission product yield · Tensor decomposition · Transport-burnup simulation · Machine learning

1 Introduction

Fission, which was discovered in 1938 [1, 2], currently plays a vital role in various science and technology fields. Because of the complexity of the fission process, the exploration of its mechanism is valuable in nuclear physics, astrophysics, and particle physics [3–8]. Furthermore, because of the large thermal energies, neutrons, and radioisotopes produced during fission, it is widely used in the energy, biology, chemistry, and medicine domains. Therefore, fission is extensively studied in the nuclear engineering and technology field for its scientific use [9].

Fission product yield (FPY) is an important observable of fission; it is generally divided into the independent and cumulative cases depending on whether the products are counted before or after the β decay, respectively. The independent fission product yield (IFPY) reflects information

This work was supported by the National Natural Science Foundation of China (Nos. 11875328, 12075327 and 12105170), the Key Laboratory of Nuclear Data foundation (No. JCKY2022201C157), the Fundamental Research Funds for the Central Universities, Sun Yat-sen University (No. 22lgqb39), and the Open Project of Guangxi Key Laboratory of Nuclear Physics and Nuclear Technology (No. NLK2020-02).

✉ Jun Su
sujun3@mail.sysu.edu.cn

Hui Guo
hui.guo@sjtu.edu.cn

[1] School of Nuclear Science and Engineering, Shanghai Jiao Tong University, Shanghai 200240, China

[2] Sino-French Institute of Nuclear Engineering and Technology, Sun Yat-sen University, Zhuhai 519082, China

on the fission process from macro and micro perspectives, which is very helpful for the research and modeling of the fission process [10]. Whereas the FPY determines the production of hundreds of radioisotopes in fission; hence, it is also an indispensable nuclear data basis for various applications of fission in nuclear engineering and technology. However, experimental measurements of the IFPY are difficult [11]. Hence, in major nuclear data libraries, such as ENDF/B [12], JEFF [13], and JENDL [14], complete evaluations of the IFPY are not available for certain actinides and are only available for three neutron incident energy points (0.0253 eV, 0.5 MeV, and 14 MeV). Therefore, a theoretical evaluation of the IFPY is still necessary.

Owing to the complexity of the quantum many-body problem and the nuclear force problem, a deep understanding and simulation of the fission process is still a challenging task in nuclear physics [3, 4]. Currently, microscopic [15–17] and macroscopic–microscopic [18–21] nuclear fission models have made significant progress in the calculation of the FPY. Phenomenological methods are widely used for practical applications that require higher precision. For example, the multi-Gaussian semi-empirical formula [10, 22], the Brosa model [23], the Gorodisskiy's method [24, 25], and the general description of fission observables (GEF) model [26] have all achieved considerable success in evaluating fission yield data. Recently, machine learning algorithms have been used in various studies in nuclear physics and nuclear techniques owing to their powerful ability to learn from existing data and perform evaluations [27–36]. To study and evaluate fission yields, Lovell et al. used mixture density networks to learn the parameters of Gaussian functions and evaluate FPYs [37]. Wang et al. evaluated the mass distribution of fission yield by combining the Bayesian neural network (BNN) and TALYS model [38]. Qiao et al. used the BNN model to evaluate the charge distribution of ^{239}Pu fission yield [39]. Tong et al. predicted neutron-induced fission-product yields by combining the k-nearest neighbor (KNN) algorithm and GEF model [40]. Recently, considering the complex multidimensional dependence and large gaps in experimental independent yield data, the tensor decomposition algorithm, which is a standard technique to capture multidimensional structural dependence [41–43], was applied to the evaluation of IFPY, and the fission yield tensor decomposition (FYTD) model was developed [44].

Most of the abovementioned studies only directly compared and verified evaluation using experimental or evaluation data. Owing to the narrow evaluation range and low evaluation accuracy, the evaluation is difficult to use in practical applications. Further, accurately evaluating the yield of hundreds of products under the fission of several dozens of target nuclei is almost impossible. Direct comparison and verification alone cannot prove whether some of the nuclides that are not accurately evaluated have a greater impact on practical applications. In this regard, this study takes advantage of the fact that the FYTD model can currently evaluate the yields of 851 fission products. Thus, this study applies its evaluation results to transport-burnup simulations to verify its performance in practical applications. Burnup or depletion is a time-dependent process by which nuclides transmute upon irradiation. Simulation of this process plays an important role in the design and licensing of nuclear reactors [45]. In a nuclear reactor, this process involves the production, transmutation, and spontaneous decay of thousands of nuclides; thus, accurate FPY data are indispensable for the simulation of this process. Moreover, hundreds of fission products in the reactor affect the reactor operation stage, spent fuel temporary storage stage, reprocessing, and long-term waste storage [46]. Therefore, this study compares the transport-burnup simulation results using the FYTD model evaluation with the reference results using ENDF/B data from various aspects to verify the evaluation results.

In this study, the transport-burnup simulation was performed using OpenMC, which is a community-developed Monte Carlo neutron and photon transport simulation code [47]. With the efforts of the community, OpenMC has implemented the burnup solver in Python and connected it with the OpenMC transport solver through a C++ interface program, thus realizing transport-burnup coupling in memory. In Ref. [48], the implementation and functions of OpenMC's depletion capabilities were elaborated and verified. The remainder of this paper is organized as follows. Section 2 describes the FYTD model [44] and OpenMC Monte Carlo transport code. Section 3 applies the FYTD model evaluation in OpenMC transport-burnup simulation for verification. Finally, Sect. 4 presents the conclusions and perspectives for future studies.

2 Theoretical framework

2.1 Fission yield tensor decomposition model

In our previous study, an FYTD model was developed [44]. In the FYTD model, first, the fission yield data are tensorized. Second, the constructed yield tensor is filled with the independent yield data of ^{227,229,232}Th, ^{231}Pa, ^{232,233,234,236,237,238}U, ^{237,238}Np, ^{238,239,240,241,242}Pu, ^{241,243}Am, and ^{242,243,245,246}Cm from the ENDF/B-VIII.0 database to obtain the missing tensor. Next, the yield tensor is decomposed into three factor matrices, and the factor matrices are iteratively updated using the Bayesian Gaussian CANDECOMP/PARAFAC (BGCP) tensor decomposition model algorithm [42]. After reconstruction of the three-factor matrices, the results are normalized to obtain the final evaluation result. A simple framework for the FYTD model is shown in Fig. 1, and details can be found

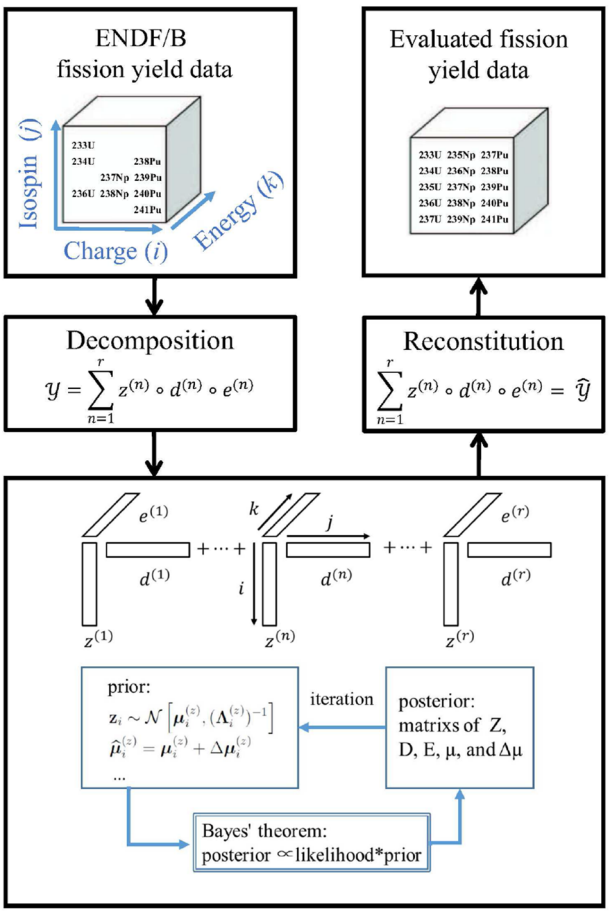

Fig. 1 (Color online) Framework of fission yield tensor decomposition (FYTD) model

in Ref. [44]. In this study, the FTYD model was used to evaluate ^{235}U and ^{239}Pu FPY. All the ^{235}U or ^{239}Pu FPY data in the ENDF/B-VIII.0 database for the three energy points (0.0253 eV, 0.5 MeV, and 14 MeV) were set as missing values, and the FYTD model was used to reproduce the ^{235}U or ^{239}Pu FPY data.

In Ref. [44], to evaluate the FYTD model quantitatively, the root mean square error (RMSE) and χ_N^2 metrics were used to measure the deviation between the evaluation and ENDF/B data. For a fission system, the RMSE is calculated by evaluating the deviation of the predicted results of the 851 products from the ENDF/B, as follows.

$$\mathrm{RMSE} = \sqrt{\frac{1}{N}\sum_{p=1}^{N}\left[\log(\widehat{Y}^p) - \log(Y^p)\right]^2}, \tag{1}$$

where $N = 851$ for 851 fission products; $\widehat{Y}^p$ represents the FYTD model evaluation of the yield of the p-th product; and Y^p represents the corresponding ENDF/B data.

For a comparison with other models and data, as defined in Ref. [38], χ_N^2 is used to measure the deviation of the predicted value of the mass distribution from the ENDF/B data, as follows.

$$\chi_N^2 = \frac{1}{N}\sum_{p=1}^{N}\left(\widehat{Y}^p - Y^p\right)^2, \tag{2}$$

where $N = 107$, which implies that the range of statistics is $A = 66$–172 for a total of 107 mass points. RMSE and χ_N^2 have different emphasis. In the calculation of RMSE, the magnitude difference between the predicted value of each product and the ENDF/B data is considered, which can globally evaluate the accuracy of the magnitude prediction. Therefore, the contribution of some products with small yield values cannot be ignored. By contrast, χ_N^2 focuses more on evaluating the accuracy of the peak area predictions.

When evaluating the fission yield data of ^{235}U, the FYTD model ($\chi_N^2 = 0.701$) agreed with the ENDF/B-VIII.0 data better than the TALYS model ($\chi_N^2 = 8.334$) and BNN+TALYS model ($\chi_N^2 = 1.134$) did; the RMSE was 0.622 for thermal neutron-induced FPYs. Furthermore, the mass distribution and isotope yields during fission were evaluated herein. For fast neutron-induced fission of ^{239}Pu, as evidently from Fig. 2, 98% of the evaluations of the isotope yields by the FYTD model agreed with the ENDF/B-VIII.0 data within 1 order of magnitude, and the RMSE was 0.395. Overall, the larger the yield, the more accurate the evaluation, which is beneficial for practical applications in reactor physics. These direct comparisons further revealed that some FPYs still had large errors. Whether these products affect the the reactor physics simulation is unknown. The transport-burnup process in a reactor is quite complex and involves thousands of nuclides and their possible transmutation or decay. The concentration of nuclides may depend on the fission yields of the various products. These errors may accumulate or weaken during these processes. Theoretically analyzing these errors is challenging; thus, systematic and macro-level verification is required. In addition, the focus of reactor physics is different from that of nuclear physics, and minor changes in the concentration of some important products have a great impact; by contrast, less attention may be paid to the concentration of some nuclides. Therefore, to perform a macro-level verification, the evaluated FPY data of ^{235}U or ^{239}Pu were applied in the transport-burnup simulation in this study.

2.2 Transport-burnup calculation method

Currently, the continuous energy (CE) transport-burnup calculation scheme has been implemented in numerous codes by coupling burnup calculations with Monte Carlo CE transport calculations, such as MCNP6 [49], Serpent [50], RMC [51], Shift [52], and OpenMC [48]. In this type of scheme, the nuclear reaction rates in depletable zones,

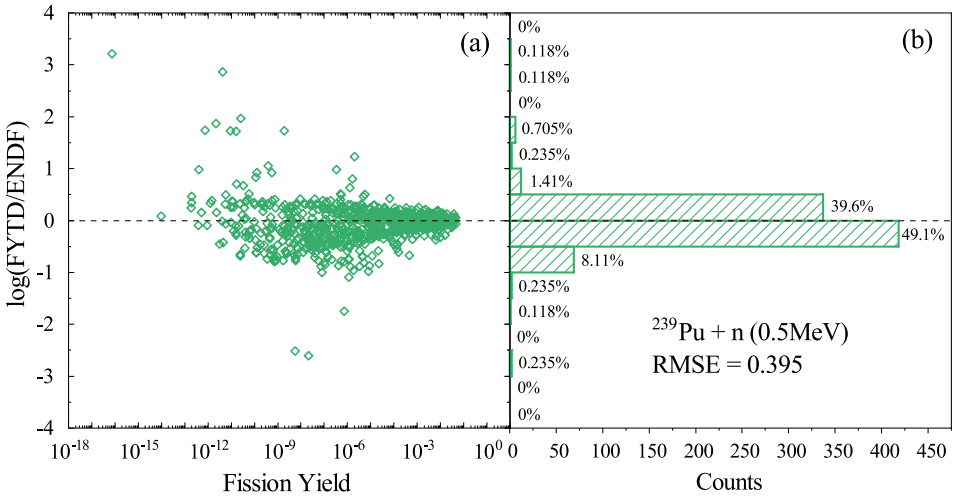

Fig. 2 (Color online) Difference between FYTD evaluation and ENDF/B-VIII.0 data for fast neutron induced ^{239}Pu fission; this figure is taken from Ref. [44]

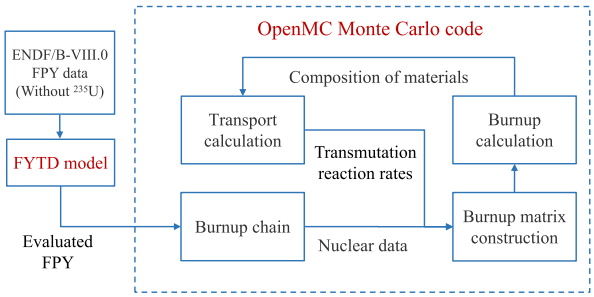

Fig. 3 (Color online) Theoretical framework of this work

which determine the rate at which nuclides are transmuted, are scored in the transport calculation and then used to solve the Bateman equations in burnup calculation. Compared with the burnup calculation coupling the deterministic neutron transport method [53–55], as the physic effects and geometry structure are intricately modeled, the Monte Carlo CE scheme is advantageous in terms of simulation accuracy. Further, it is well suited to paying attention to the details in transport-burnup simulation [52, 56–58]. Therefore, OpenMC was used in this study.

Figure 3 presents the theoretical framework of this study. In OpenMC, the depletion is inherently linked to the neutron transport equation. In the presence of an initial nuclide concentration, the transmutation reaction rate of each nuclide can be obtained by transport calculations. The burnup matrix of the burnup equation is constructed by combining the transmutation reaction rate and nuclear data (transmutation, decay, and FPY data) in the burnup chain. Conversely, obtaining new nuclide concentration data after solving the burnup equation affects the solution of the transport equation in the next step.

The ENDF-6 format [59] is a common international nuclear data format; major nuclear databases provide nuclear data in this format. OpenMC can read fission yield data in this standard format and generate a burnup chain file. In this study, the FPY data evaluated by the FYTD model were converted to the ENDF-6 format according to the requirements of the ENDF-6 manual [59]. Thus, no more changes in the OpenMC were required. The FPY data evaluated by FYTD model can be used in transport-burnup calculations using the original ENDF-6 format interface of OpenMC.

2.3 Benchmark cases

Two different reactors were selected to verify the FPY data. To verify the ^{235}U FPY and ^{239}Pu FPY, an AP1000 PWR [60] and MOX-3600 SFR [61] were adopted, respectively. At present, the PWR is widely used commercially worldwide, and the SFR is one of the most promising commercial reactors. These two reactor types have typical characteristics (one neutron spectrum of these two reactors is the thermal spectrum and the other is the fast spectrum); further, they used the UOX and MOX fuels, respectively. In Fig. 4, the calculation by OpenMC shows that the fission in the PWR over the entire 1620 effective full power days (EFPDs) is dominated by thermal neutron-induced fission, which is contributed primarily by ^{235}U. Whereas the fission in SFR over 2050 EFPDs is dominated by fast neutron-induced fission, which is contributed primarily by ^{239}Pu. Therefore, the transport-burnup simulations of these two reactions are suitable for verifying the evaluated ^{235}U and ^{239}Pu FPY, respectively.

Simultaneously, to amplify the difference caused by the difference in FPY data, instead of the full-core simulation, a single pin-cell simulation was performed. The selection of a simple single pin-cell model is conducive for eliminating the interference of other factors in the core and reducing

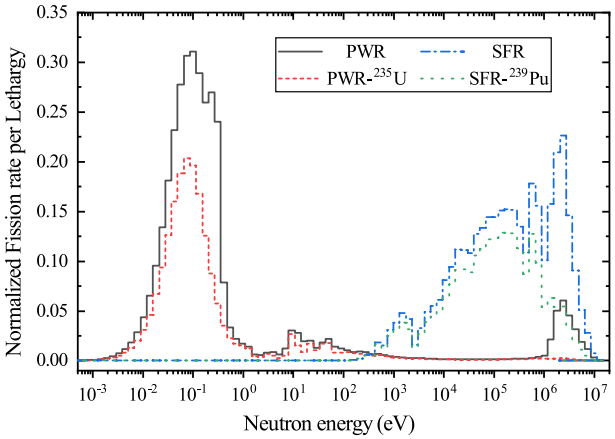

Fig. 4 (Color online) Energy distribution of fission reactions in a pressurized water reactor (PWR) and sodium-cooled fast reactor (SFR)

the complexity of the analysis. Thus, more attention can be paid to the influence of different original nuclear data. The geometric models of the two types of reactor pin-cells and the parameters used in the OpenMC burnup calculation are presented in Fig. 5 and Table 1, respectively. In this study, the method of calculating the average FPY in OpenMC was applied to treat the energy dependence of FPY. The average energy at which fission events occur was tallied in the transport calculation and used to calculate an effective FPY by linear interpolation. Subsequently, the effective average FPY was used in the burnup calculation.

Finally, verification in this study was not performed by comparison with the experimental data. Note that the experimental data of reactor physics involve various complex factors, such as shutdown and restart during reactor operation. Further, the restoration of these processes in the simulation

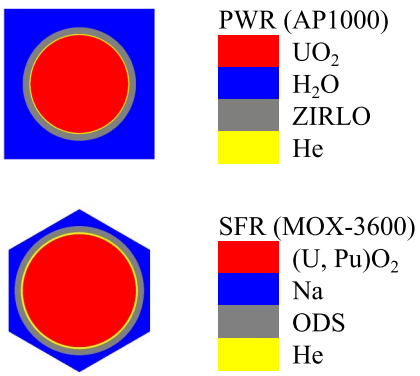

Fig. 5 (Color online) Pin-cell models for the PWR (AP1000) and SFR (MOX-3600)

Table 1 OpenMC transport-burnup calculation parameters for different reactors

	PWR (AP1000)	SFR (MOX-3600)
Line power density	187.7 W/cm	291.6 W/cm
Burnup depth	540 × 3 EFPD	410 × 5 EFPD
	62 GWd/tHN	97 GWd/tHN
Calculation step	54 EFPD	205 EFPD

is complex, and the resulting errors are inevitable. Thus, in the final comparison, determining whether the error was caused by the yield data or other factors is impossible. Therefore, by only changing the yield data, two calculations were performed. Thus, the impact of the yield data could be directly observed and the accuracy of the evaluated yield data could be better evaluated. Moreover, the experimental data of FPY are not systematic, and applying it directly to the burnup calculation is impossible. Therefore, burnup calculations were performed twice: once using the FPY in the ENDF/B-VIII.0 database, and once using the FPY evaluated by the FYTD model. The accuracy of the evaluation results was assessed by calculating the error between these two calculations.

3 Results and discussion

To verify the evaluated neutron-induced FPY in practical applications, all the ^{235}U and ^{239}Pu yields under the three energy points were set as missing values, and the FYTD model was used to reproduce the ^{235}U or ^{239}Pu yield data. All burnup calculations were performed twice: once using the fission yield data of ^{235}U or ^{239}Pu in the ENDF/B-VIII.0 database, and once using the fission yield data of ^{235}U evaluated by the FYTD model; and all rest parameters and nuclear data remained the same. The burnup calculation results using the ENDF/B-VIII.0 data were regarded as the reference results and are denoted by a red dotted line in the subsequent figures. The burnup calculation results using the evaluated FPY are denoted by black dotted lines. The difference between these and reference results are denoted by the green dots. Note that the smaller the difference, the more accurate the evaluation. For convenience of presentation, ENDF/B-VIII.0 is abbreviated as ENDF/B in the following text and figures.

The impacts of fission products on reactors and fuels are multifaceted. During reactor operation, neutron poisons in the fission products affect the reactivity of the reactor. Simultaneously, the variations in concentration of neutron poisons in a reactor shutdown for several hours to several days also affect the restart of the reactor. The short-lived fission products have strong radioactivity and decay heat; thus,

the spent fuel must be stored for several years after being out of the reactor to reduce their impact. Medium-lived and long-lived fission products affect the subsequent reprocessing and long-term disposal of radioactive waste. Therefore, the comparison herein was performed step-by-step from the reactor operation stage, spent fuel temporary storage stage, reprocessing, and long-term waste storage stage to verify the accuracy of the evaluated FPY data in various scenarios.

3.1 Reactor operation stage

The first comparison is the variation in the neutron effective multiplication factor k_{eff} with burnup. With increasing burnup, fissionable nuclides are gradually consumed, and fission products are gradually accumulated. These processes have a significant impact on reactor reactivity, which requires attention during reactor operation. Evidently from Fig. 6a, compared with the reference results, the PWR k_{eff} calculated using the FYTD model evaluation was slightly underestimated, and the degree of underestimation was within 500 pcm over 1620 EFPDs. The variation in reactivity was as high as tens of thousands of pcm over 1620 EFPDs. By contrast, the degree of underestimation was not significant. For the SFR in Fig. 6b, the difference was within 200 pcm over 2050 EFPDs.

To explore the sources of the differences shown in Fig. 6, the macroscopic neutron radiative capture cross-section of the time point with the largest error was calculated and is presented in Tables 2 and 3. These two tables list the 20 nuclides that contribute the most to neutron radiation capture in the reactor and the sum of the macroscopic neutron radiative capture cross-sections of all nuclides. Evidently from Table 2, for the PWR, the total macroscopic thermal neutron radiative capture cross-section was overestimated by 0.75% owing to the accumulation of calculation errors in various nuclides, for example, ^{135}Xe, ^{151}Sm, ^{103}Rh, and ^{153}Eu. Because of this overestimation, k_{eff} was underestimated by 417 pcm at 864 EFPDs in Fig. 6. Evidently from Table 3, for the SFR, the contribution of fission products was smaller than that in the PWR, and the impact of their errors was relatively weak. However, the underestimation of ^{105}Pd, ^{103}Rh, ^{107}Pd, and other products ultimately led to an underestimation of 0.18% of the total macroscopic fast neutron radiative capture cross section, thus resulting in an overestimation of 171 pcm of k_{eff} at 1620 EFPDs, as shown in Fig. 6.

For more intuitive and effective comparison and verification, the subsequent comparisons focused on the key fission products. For the operation stage of the PWR, ^{135}Xe is one of the most important fission products, and its thermal neutron absorption cross section is as high as 2,650,000 barns. Its accumulation in the reactor significantly affects

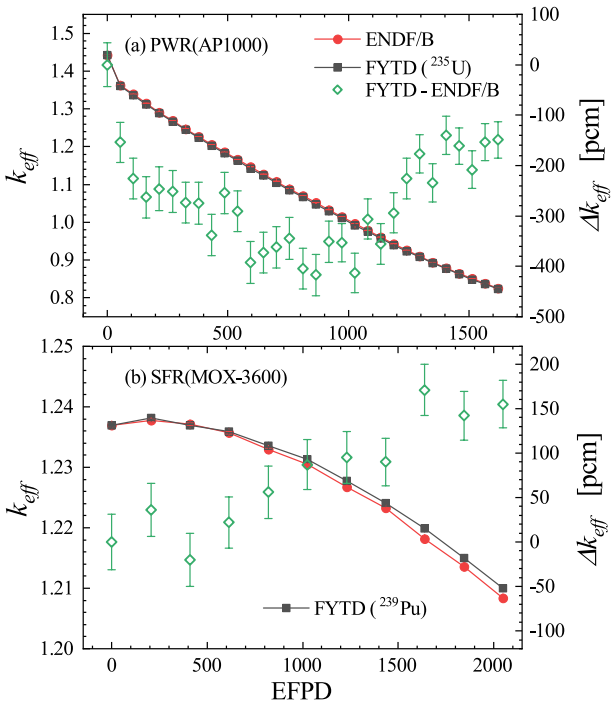

Fig. 6 (Color online) Variations of k_{eff} with burnup for (**a**) PWR and (**b**) SFR

Table 2 Macroscopic thermal neutron radiative capture cross-section in AP1000 at 864 effective full power days (EFPDs)

Nuclide	Contribution (%)	ENDF/B (cm^{-1})	FYTD (cm^{-1})	Difference (%)
^{238}U	27.38	5.87×10^{22}	5.87×10^{22}	0.00
^{235}U	15.17	3.25×10^{22}	3.25×10^{22}	0.07
^{239}Pu	14.62	3.13×10^{22}	3.14×10^{22}	0.26
^{135}Xe	9.90	2.12×10^{22}	2.14×10^{22}	0.95
^{240}Pu	6.04	1.29×10^{22}	1.30×10^{22}	0.14
^{143}Nd	5.18	1.11×10^{22}	1.08×10^{22}	− 3.07
^{241}Pu	4.07	8.73×10^{21}	8.75×10^{21}	0.15
^{151}Sm	2.90	6.21×10^{21}	6.52×10^{21}	5.06
^{149}Sm	1.61	3.45×10^{21}	3.41×10^{21}	− 1.01
^{103}Rh	1.59	3.42×10^{21}	3.61×10^{21}	5.58
^{131}Xe	0.83	1.77×10^{21}	1.89×10^{21}	6.73
^{237}Np	0.75	1.61×10^{21}	1.61×10^{21}	0.41
^{133}Cs	0.68	1.46×10^{21}	1.51×10^{21}	3.44
^{147}Pm	0.66	1.41×10^{21}	1.35×10^{21}	− 4.11
^{153}Eu	0.64	1.38×10^{21}	1.56×10^{21}	13.14
^{145}Nd	0.55	1.19×10^{21}	1.10×10^{21}	− 6.90
^{150}Sm	0.51	1.08×10^{21}	1.07×10^{21}	− 0.89
^{238}Pu	0.48	1.03×10^{21}	1.03×10^{21}	0.31
^{155}Eu	0.47	1.01×10^{21}	1.16×10^{21}	14.93
^{105}Rh	0.46	9.84×10^{20}	1.05×10^{21}	6.86
Others	5.50	1.18×10^{22}	1.25×10^{22}	6.03
Total	100.00	2.143×10^{23}	2.159×10^{23}	0.75

Table 3 Macroscopic fast neutron radiative capture cross-section in MOX-3600 at 1640 EFPDs

Nuclide	Contribution (%)	ENDF/B (cm^{-1})	FYTD (cm^{-1})	Difference (%)
^{238}U	71.57	1.80×10^{21}	1.80×10^{21}	0.00
^{239}Pu	8.46	2.12×10^{20}	2.12×10^{20}	0.00
^{240}Pu	5.52	1.39×10^{20}	1.39×10^{20}	0.02
^{242}Pu	1.45	3.64×10^{19}	3.64×10^{19}	0.00
^{241}Am	1.18	2.96×10^{19}	2.96×10^{19}	− 0.01
^{241}Pu	0.87	2.19×10^{19}	2.19×10^{19}	0.01
^{243}Am	0.78	1.95×10^{19}	1.95×10^{19}	0.03
^{105}Pd	0.71	1.78×10^{19}	1.54×10^{19}	− 13.53
^{238}Pu	0.63	1.57×10^{19}	1.57×10^{19}	− 0.01
^{99}Tc	0.61	1.53×10^{19}	1.56×10^{19}	1.62
^{101}Ru	0.59	1.49×10^{19}	1.43×10^{19}	− 3.74
^{133}Cs	0.56	1.41×10^{19}	1.39×10^{19}	− 1.14
^{103}Rh	0.55	1.38×10^{19}	1.30×10^{19}	− 6.07
^{107}Pd	0.39	9.72×10^{18}	9.02×10^{18}	− 7.20
^{149}Sm	0.35	8.68×10^{18}	8.55×10^{18}	− 1.57
^{97}Mo	0.34	8.46×10^{18}	8.67×10^{18}	2.45
^{102}Ru	0.33	8.40×10^{18}	8.26×10^{18}	− 1.64
^{147}Pm	0.26	6.61×10^{18}	6.92×10^{18}	4.69
^{95}Mo	0.26	6.55×10^{18}	6.58×10^{18}	0.49
^{16}O	0.25	6.37×10^{18}	6.37×10^{18}	0.00
Others	4.33	1.09×10^{20}	1.08×10^{20}	− 0.43
Total	100.00	2.51×10^{21}	2.50×10^{21}	− 0.18

the reactivity of the reactor. A small part of ^{135}Xe in the reactor is directly generated by fission, whereas most of ^{135}Xe is produced by the decay of ^{135}I. Therefore, the concentration of ^{135}Xe in the reactor is directly affected by the independent yield of ^{135}Xe and ^{135}I and its parents. In the several hours after the shutdown of a PWR, owing to the sharp reduction of neutron flux, the concentration of ^{135}Xe varies sharply, and this short-term variation affects the restart of the reactor. Therefore, from the perspective of the actual operation of the reactor, the variation in ^{135}Xe concentration in the PWR was calculated over 72 h of shutdown after 1080 EFPDs. Evidently from Fig. 7b, ^{135}Xe first increased to the maximum value, and then gradually decreased, thus exhibiting a distinct iodine pit phenomenon. During the period of the iodine pit, a forced shutdown time may occur because of the high concentration of ^{135}Xe, and the reactor cannot be restarted. Therefore, the concentration of ^{135}Xe during this period is very important. Evidently, the two results were similar; over these 72 h, the difference was within ±1%. This is primarily because the FYTD model can accurately evaluate the independent yield of ^{135}I and ^{135}Xe in thermal neutron induced ^{235}U fission.

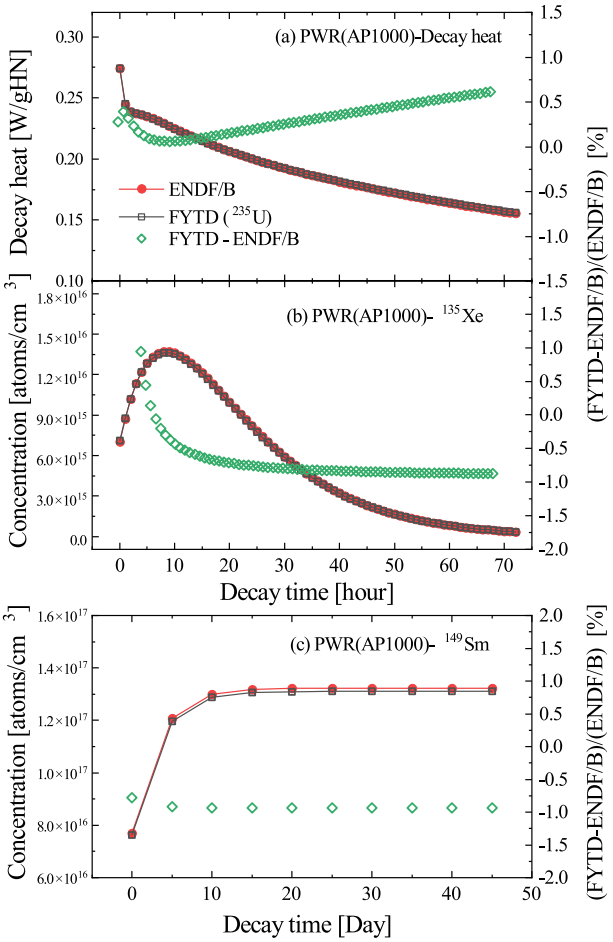

Fig. 7 (Color online) Variations in (**a**) fuel decay heat and (**b**) ^{135}Xe concentration in the PWR over 72 h of shutdown; and variation in (**b**) ^{149}Sm concentration over 45 days of shutdown

During the short-term shutdown period, the removal of decay heat of the reactor is another important issue, and the decay heat at this time is contributed primarily by short-lived and highly radioactive fission products. Figure 7a shows the variation in fuel decay heat within 72 h of shutdown. Evidently, the results using the FYTD model evaluation were still very close to the reference results, with a difference of no more than ±1% in the entire period. This indirectly proves that the FYTD model can evaluate the large yields of short-lived fission products, such as ^{131}I and ^{140}Ba.

Similar to ^{135}Xe, ^{149}Sm is also an important fission product that affects reactivity. However, unlike ^{135}Xe, the concentration variation of ^{149}Sm is relatively simple because ^{149}Sm itself does not decay and the half-life of its parent nucleus ^{149}Pm is longer than ^{135}I; thus, its concentration variation rate is slower and the trend is more uniform. To compare the accumulation of ^{149}Pm, a period of 45 days of refueling overhaul after 1080 EFPDs of AP1000 operation was simulated. During this period, ^{149}Pm continued to accumulate

in the reactor, and when the reactor was restarted after the refueling overhaul, it resulted in a certain negative reactivity to the reactor. Evidently from Fig. 7c, the accumulation of ^{149}Sm had a small difference from the reference result and was within ±1%.

3.2 Temporary storage of spent fuel

After 1620 EFPDs of AP1000 operation and 2050 EFPDs of MOX-3600 operation, the fuel is unloaded from the reactor and placed in a spent fuel storage pit for years to cool. Currently, temporary storage is widely used. The spent fuel that has just been released from the reactor contains a large amount of short-lived fission products, and the radioactivity and decay heat are extremely high. During the cooling process of the spent fuel, fission products with short half-lives gradually decay, and the heat generated is removed by water. Therefore, during temporary storage for several years, the activity and decay heat of spent fuel, which are contributed primarily by short-lived fission products, deserve attention. To this end, simulations of the decay process of spent fuel 3 years after leaving the reactor were performed focusing on the behavior of spent fuel in the pool. Evidently from Figs. 8 and 9, for both the PWR and SFR, the differences in decay heat and activity over these 3 years were within ±2%.

Reprocessing of spent fuel is possible only after the fuel has been cooled for several years, thereby reducing the radioactivity and heat production to a certain level. Although the radioactivity, contributed primarily by ^{137}Cs and ^{90}Sr, is considerably reduced at this time, it is still an important factor that cannot be ignored in the reprocessing process.

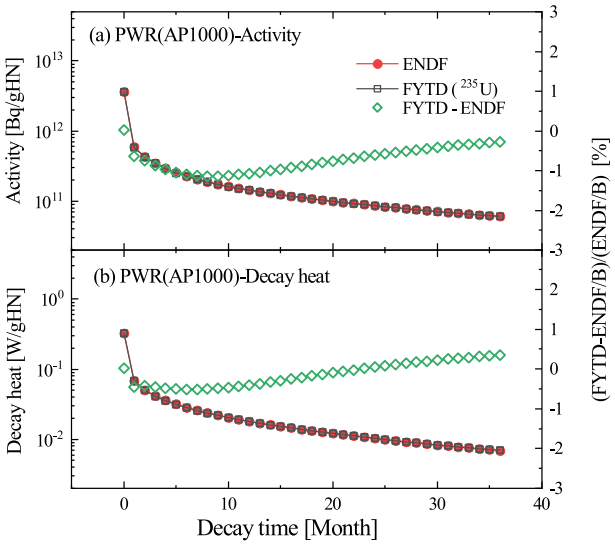

Fig. 8 (Color online) Variations in (**a**) activity and (**b**) decay heat of PWR spent fuel over 3 years of temporary storage

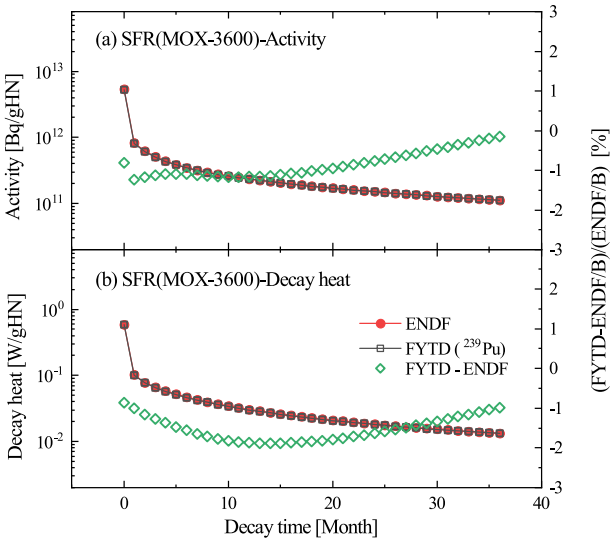

Fig. 9 (Color online) Variations in (**a**) activity and (**b**) decay heat of SFR spent fuel over 3 years of temporary storage

In addition, ^{90}Sr is the most biologically harmful nuclide in spent fuels. In addition, other types of nuclides, such as fission gases, also deserve attention in reprocessing. ^{85}Kr is the only radioactive fission gas that is present in large quantities after years of spent fuel cooling and is released from spent fuel during shearing. After a certain treatment, it is released into the atmosphere. Therefore, taking these three nuclides as examples, this study focused on the concentration variations and accumulation of some nuclides that are important for reprocessing. Figure 10 shows the variations in concentration of ^{137}Cs, ^{90}Sr, and ^{85}Kr within 3 years of cooling; the errors from the reference results were approximately 1%, 3%, and 6%, respectively.

3.3 Reprocessing and long term disposal

After the mainstream reprocessing at this stage was completed, heavy nuclei, such as U and Pu, were separated, and 99.9% of the fission products were processed and entered high-level liquid waste (HLLW). HLLW still needs to be stored in tanks for 30 years to reduce the radioactivity and decay heat before solidification. Within 30 y, as the heavy nuclei were separated, the amount of interest changed from the activity and decay heat of the entire spent fuel to the activity and decay heat contributed solely by fission products. Assuming that the activity and decay heat of HLLW are all contributed by fission products, Fig. 11 shows the calculated activity and decay heat of HLLW within 30 years; evidently, the difference was within ±1.5%. Because the effect of heavy nuclear decay was removed from this comparison

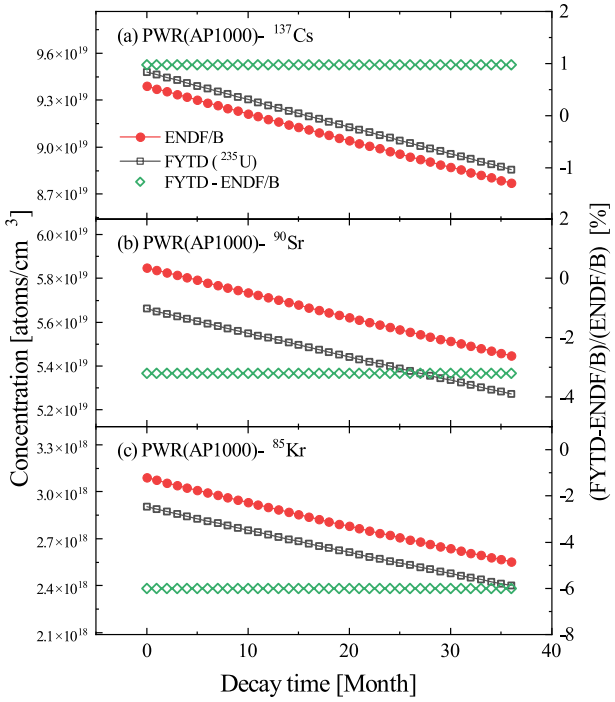

Fig. 10 (Color online) Variations in (**a**) ^{137}Cs, (**b**) ^{90}Sr, and (**c**) ^{85}Kr concentrations in PWR spent fuel over 3 years of temporary storage

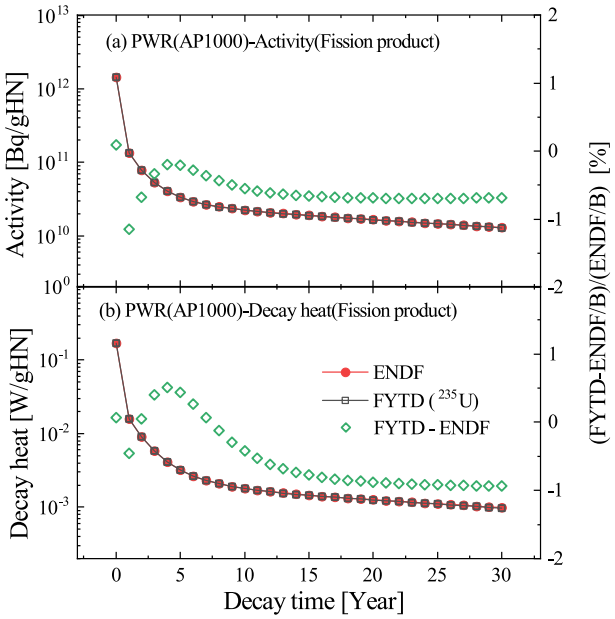

Fig. 11 (Color online) Variations in (**a**) activity and (**b**) decay heat of high-level liquid waste over 30 years of storage

of the decay heat and activity, it could better demonstrate the accuracy of FPY evaluations.

After 30 years of storage, HLLW can undergo solidification treatment and deep geological disposal. In addition to solidified HLLW, other types of radioactive waste, such as silver adsorbents that adsorb ^{129}I, require deep geological disposal. Geological disposal can last for thousands or tens of thousands of years. At this time, the focus is on the seven longest-lived fission products (LLFP), ^{99}Tc, ^{126}Sn, ^{79}Se, ^{93}Zr, ^{107}Pd, ^{135}Cs, and ^{129}I. Among them, ^{129}I and ^{99}Tc are strong biological hazards. Evidently from Fig. 12, the evaluation of ^{99}Tc by the FYTD model was still very accurate, with a difference of approximately 2% from the benchmark result. However, the results of ^{129}I were different from those of the benchmark, with a difference of approximately 37%. This is because the independent yield of ^{129}I in the thermal neutron-induced ^{235}U fission in the ENDF/B-VIII.0 database is 0, and the accumulation of ^{129}I in the reactor is due to the decay of another product with mass 129. However, mass 129 is at the junction of the heavy nucleus peak and valley area in the FPY mass distribution, where the yield varies significantly, and the evaluation here is difficult. Thus, the FYTD evaluation at mass 129 deviated from the ENDF/B data.

The above comparison and verification were aimed primarily at the reprocessing of the PWR, which is different from that of the SFR. Reprocessing is indispensable for the development of fast reactor because it is related to their fuel cycle process. The separation of additional fission products is being considered in a variety of advanced reprocessing processes. For example, ^{137}Cs and ^{90}Sr, two highly radioactive medium-lived fission products, are not considered for separation in the current process but are disposed of as high-level radioactive wastes. In future reprocessing processes, they will

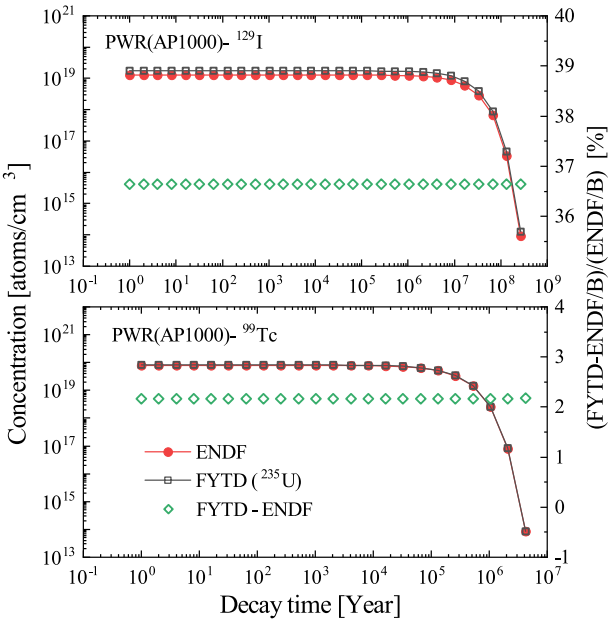

Fig. 12 (Color online) Variations in (**a**) ^{129}I and (**b**) ^{99}Tc concentrations in PWR spent fuel over millions of years

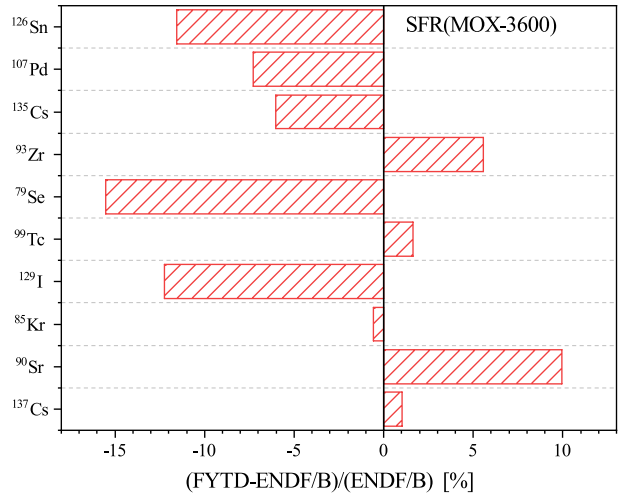

Fig. 13 (Color online) Comparison of cumulative concentration after 3 years of temporary storage for several nuclides in SFR spent fuel

be considered separately for medical use. In addition, the seven LLFPs are not separated in the current reprocessing process and are ultimately disposed of in geology. These nuclides are extremely long-lived, and the hazards they will cause during deep geological disposal over the next tens of thousands of years are difficult to estimate. Thus, scientists are considering using fast reactors or accelerator-driven subcritical systems (ADSs) to transmutate them. Therefore, in the advanced reprocessing process, these long-lived fission products will be separated and returned to the fast reactor or ADS for transmutation. The accumulation of these long-lived fission products is important at this point and is a concern for subsequent transmutation processes. Therefore, the accumulation of some of the above important nuclides was calculated after cooling for 3 years and before the reprocessing process. Figure 13 shows the comparison of these nuclide accumulations. Evidently, the evaluations of ^{99}Tc, ^{137}Cs, and ^{85}Kr were relatively accurate, and the differences from the reference values were all within ±2%. They were followed by ^{135}Cs, ^{107}Pd, ^{93}Zr, and ^{90}Sr, the results of which had slightly larger errors, ranging from ±5% to ±10%. Further, the evaluations for ^{126}Sn, ^{79}Se, and ^{129}I were less accurate, with errors within ±15%. These three nuclides were located at $A = 79$, 126, 129, at the edge of the light-nuclear peak or the heavy-nuclear peak in the mass distribution. The yield values here were smaller and more variable; thus, the evaluations were not sufficiently accurate. However, several LLFPs were located in these regions. Therefore, if the evaluation using FYTD models is to be applied to the accurate study of LLFPs, further improvements to the model are required.

4 Conclusion

In this study, an FYTD model was used to evaluate the IFPY. The evaluated FPYs were applied in the OpenMC transport-burnup simulation of a PWR and SFR for verification. By comparing the transport-burnup simulation results using the FYTD model evaluation with the reference results using ENDF/B data, the performance of the evaluation data in a real application was examined.

First, for the reactor operation stage, the variation in k_{eff} was calculated. For the pin-cell of the PWR, the errors in reactivity caused by the evaluated FPY did not exceed 500 pcm over 1620 EFPDs, and did not exceed 150 pcm for the SFR pin-cell over 2050 EFPDs. The errors in decay heat, and the ^{135}Xe and ^{149}Sm concentrations during the short-term shutdown of the PWR were all less than 1%. Second, the decay heat and activity of the spent fuel during the 3 years of temporary storage were calculated. For both the PWR and SFR, the decay heat and activity errors were less than 2%. Finally, for reprocessing and long-term waste storage, the concentrations of important nuclides and the activity and decay heat of HLLW were calculated. For the PWR, the errors in the concentration of important nuclides in the spent fuel, such as ^{90}Sr, ^{137}Cs, ^{85}Kr, and ^{99}Tc, were less than 6%. Further, the errors in the activity and decay heat of the HLLW were less than 1.5% over 30 years of canned storage. For the SFR, the concentration errors of the 10 important nuclides in the spent fuel were all less than 16%.

Multiple rounds of comparative verification for the reactor operation stage, spent fuel temporary storage stage, reprocessing, and long-term waste storage revealed that the transport-burnup simulation results using the FYTD model evaluation exhibited little difference with the reference results using ENDF/B-VIII.0. This proves that the evaluation of the FYTD model may have application value for reactor physical analysis.

Author contributions Jun Su contributes comparably to the conceptualization and funding acuisition. Hui Guo contributes comparably to the conceptualization and funding acuisition. Qufei Song contributes mainly to investigation, methodology, resources, original draft writing, and review eding writing. Long Zhu contributes secondary to the original draft writing.

References

1. O. Hahn, F. Strassmann, Über den nachweis und das verhalten der bei der bestrahlung des urans mittels neutronen entstehenden erdalkalimetalle. Naturwissenschaften **27**, 11–15 (1939). https://doi.org/10.1007/BF01488241
2. L. Meitner, O.R. Frisch, Disintegration of uranium by neutrons: a new type of nuclear reaction. Nature **143**, 239–240 (1939). https://doi.org/10.1038/143239a0

3. N. Schunck, L. Robledo, Microscopic theory of nuclear fission: a review. Rep. Prog. Phys. **79**, 116301 (2016). https://doi.org/10.1088/0034-4885/79/11/116301
4. M. Bender, R. Bernard, G. Bertsch et al., Future of nuclear fission theory. J. Phys. G Nucl. Part. Phys. **47**, 113002 (2020). https://doi.org/10.1088/1361-6471/abab4f
5. J. Hamilton, S. Hofmann, Y. Oganessian, Search for superheavy nuclei. Annu. Rev. Nucl. Part. Sci. **63**, 383–405 (2013). https://doi.org/10.1146/annurev-nucl-102912-144535
6. J.C. Pei, W. Nazarewicz, J.A. Sheikh et al., Fission barriers of compound superheavy nuclei. Phys. Rev. Lett. **102**, 192501 (2009). https://doi.org/10.1103/PhysRevLett.102.192501
7. M. Eichler, A. Arcones, A. Kelic et al., The role of fission in neutron star mergers and its impact on the r -process peaks. Astrophys. J. **808**, 30 (2015). https://doi.org/10.1088/0004-637X/808/1/30
8. T.A. Mueller, D. Lhuillier, M. Fallot et al., Improved predictions of reactor antineutrino spectra. Phys. Rev. C **83**, 054615 (2011). https://doi.org/10.1103/PhysRevC.83.054615
9. L.A. Bernstein, D.A. Brown, A.J. Koning et al., Our future nuclear data needs. Annu. Rev. Nucl. Part. Sci. **69**, 109–136 (2019). https://doi.org/10.1146/annurev-nucl-101918-023708
10. D. Ramos, M. Caamaño, F. Farget et al., Insight into excitation energy and structure effects in fission from isotopic information in fission yields. Phys. Rev. C **99**, 024615 (2019). https://doi.org/10.1103/PhysRevC.99.024615
11. H.O. Denschlag, Independent fission yield measurements. Nucl. Sci. Eng. **94**, 337–352 (1986). https://doi.org/10.13182/NSE86-A18345
12. D. Brown, M. Chadwick, R. Capote et al., Endf/b-viii.0: the 8th major release of the nuclear reaction data library with cielo-project cross sections, new standards and thermal scattering data. Nucl. Data Sheets **148**, 1–142 (2018). https://doi.org/10.1016/j.nds.2018.02.001
13. A.J. Plompen, O. Cabellos, C. De Saint Jean et al., The joint evaluated fission and fusion nuclear data library, JEFF-3.3. Eur. Phys. J. A **56**, 181 (2020). https://doi.org/10.1140/epja/s10050-020-00141-9
14. K. Shibata, O. Iwamoto, T. Nakagawa et al., JENDL-4.0: a new library for nuclear science and engineering. J. Nucl. Sci. Technol. **48**, 1–30 (2011). https://doi.org/10.1080/18811248.2011.9711675
15. A. Bulgac, P. Magierski, K.J. Roche et al., Induced fission of Pu 240 within a real-time microscopic framework. Phys. Rev. Lett. **116**, 122504 (2016). https://doi.org/10.1103/PhysRevLett.116.122504
16. D. Regnier, N. Dubray, N. Schunck et al., Fission fragment charge and mass distributions in ^{239}Pu (n, f) in the adiabatic nuclear energy density functional theory. Phys. Rev. C **93**, 054611 (2016). https://doi.org/10.1103/PhysRevC.93.054611
17. W. Younes, D.M. Gogny, J.F. Berger, *A microscopic theory of fission dynamics based on the generator coordinate method*, vol. 950 (Springer, Berlin, 2019)
18. J. Randrup, P. Möller, Brownian shape motion on five-dimensional potential-energy surfaces: nuclear fission-fragment mass distributions. Phys. Rev. Lett. **106**, 132503 (2011). https://doi.org/10.1103/PhysRevLett.106.132503
19. J. Randrup, P. Möller, A.J. Sierk, Fission-fragment mass distributions from strongly damped shape evolution. Phys. Rev. C **84**, 034613 (2011). https://doi.org/10.1103/PhysRevC.84.034613
20. K. Pomorski, F.A. Ivanyuk, B. Nerlo-Pomorska, Mass distribution of fission fragments within the Born–Oppenheimer approximation. Eur. Phys. J. A **53**, 59 (2017). https://doi.org/10.1140/epja/i2017-12250-5
21. L.L. Liu, X.Z. Wu, Y.J. Chen et al., Study of fission dynamics with a three-dimensional Langevin approach. Phys. Rev. C **99**, 044614 (2019). https://doi.org/10.1103/PhysRevC.99.044614
22. Z.X. Fang, M. Yu, Y.G. Huang et al., Theoretical analysis of long-lived radioactive waste in pressurized water reactor. Nucl. Sci. Tech. **32**, 72 (2021). https://doi.org/10.1007/s41365-021-00911-0
23. U. Brosa, S. Grossmann, A. Müller, Nuclear scission. Phys. Rep. **197**, 167–262 (1990). https://doi.org/10.1016/0370-1573(90)90114-H
24. D. Gorodisskiy, K. Kovalchuk, S. Mulgin et al., Systematics of fragment mass yields from fission of actinide nuclei induced by the 5–200 mev protons and neutrons. Ann. Nucl. Energy **35**, 238–245 (2008). https://doi.org/10.1016/j.anucene.2007.06.002
25. M. Pahlavani, P. Mehdipour, Product yields for the photofission of ^{232}Th, ^{234,238} U, ^{237}Np, and ^{239,240,242} Pu actinides at various incident photon energies. Nucl. Sci. Tech. **29**, 146 (2018). https://doi.org/10.1007/s41365-018-0482-1
26. K.H. Schmidt, B. Jurado, C. Amouroux et al., General description of fission observables: GEF model code. Nucl. Data Sheets **131**, 107–221 (2016). https://doi.org/10.1016/j.nds.2015.12.009
27. Z. Niu, H. Liang, Nuclear mass predictions based on Bayesian neural network approach with pairing and shell effects. Phys. Lett. B **778**, 48–53 (2018). https://doi.org/10.1016/j.physletb.2018.01.002
28. L. Neufcourt, Y. Cao, W. Nazarewicz et al., Neutron drip line in the Ca region from Bayesian model averaging. Phys. Rev. Lett. **122**, 062502 (2019). https://doi.org/10.1103/PhysRevLett.122.062502
29. C.W. Ma, D. Peng, H.L. Wei et al., Isotopic cross-sections in proton induced spallation reactions based on the Bayesian neural network method. Chin. Phys. C **44**, 014104 (2020). https://doi.org/10.1088/1674-1137/44/1/014104
30. Z.P. Gao, Y.J. Wang, H.L. Lü et al., Machine learning the nuclear mass. Nucl. Sci. Tech. **32**, 109 (2021). https://doi.org/10.1007/s41365-021-00956-1
31. Q. Song, L. Zhu, J. Su, Target dependence of isotopic cross sections in the spallation reactions ^{238} U+ p, d and ^{9} Be at 1a gev. Chin. Phys. C. **46**, 074108 (2022). https://doi.org/10.1088/1674-1137/ac6249
32. E. Alhassan, D. Rochman, A. Vasiliev et al., Iterative bayesian monte carlo for nuclear data evaluation. Nucl. Sci. Tech. **33**, 50 (2022). https://doi.org/10.1007/s41365-022-01034-w
33. H. Arahmane, E.M. Hamzaoui, Y. Ben Maissa et al., Neutron-gamma discrimination method based on blind source separation and machine learning. Nucl. Sci. Tech. **32**, 18 (2021). https://doi.org/10.1007/s41365-021-00850-w
34. Z.H. Wu, J.J. Bai, D.D. Zhang et al., Statistical analysis of helium bubbles in transmission electron microscopy images based on machine learning method. Nucl. Sci. Tech. **32**, 54 (2021). https://doi.org/10.1007/s41365-021-00886-y
35. T.S. Shang, J. Li, Z.M. Niu, Prediction of nuclear charge density distribution with feedback neural network. Nucl. Sci. Tech. **33**, 153 (2022). https://doi.org/10.1007/s41365-022-01140-9
36. B.C. Wang, M.T. Qiu, W. Chen et al., Machine learning-based analyses for total ionizing dose effects in bipolar junction transistors. Nucl. Sci. Tech. **33**, 131 (2022). https://doi.org/10.1007/s41365-022-01107-w
37. A. Lovell, A. Mohan, P. Talou et al., Constraining fission yields using machine learning. EPJ Web Conf. **211**, 04006 (2019). https://doi.org/10.1051/epjconf/201921104006
38. Z.A. Wang, J. Pei, Y. Liu et al., Bayesian evaluation of incomplete fission yields. Phys. Rev. Lett. **123**, 122501 (2019). https://doi.org/10.1103/PhysRevLett.123.122501

39. C.Y. Qiao, J.C. Pei, Z.A. Wang et al., Bayesian evaluation of charge yields of fission fragments of U 239. Phys. Rev. C **103**, 034621 (2021). https://doi.org/10.1103/PhysRevC.103.034621
40. L. Tong, R. He, S. Yan, Prediction of neutron-induced fission product yields by a straightforward k-nearest-neighbor algorithm. Phys. Rev. C **104**, 064617 (2021). https://doi.org/10.1103/PhysRevC.104.064617
41. J. Liu, P. Musialski, P. Wonka et al., Tensor completion for estimating missing values in visual data. IEEE Trans. Pattern Anal. Mach. Intell. **35**, 208–220 (2013). https://doi.org/10.1109/TPAMI.2012.39
42. X. Chen, Z. He, L. Sun, A Bayesian tensor decomposition approach for spatiotemporal traffic data imputation. Transp. Res. Part C Emerg. Technol. **98**, 73–84 (2019). https://doi.org/10.1016/j.trc.2018.11.003
43. X. Chen, Z. Han, Y. Wang, et al., A general model for robust tensor factorization with unknown noise. arXiv:1705.06755
44. Q. Song, L. Zhu, J. Su, et al., A tensor decomposition model for evaluating isotopic yield in neutron-induced fission. arXiv:2208.11815
45. B.R. Betzler, F. Heidet, B. Feng et al., Modeling and simulation functional needs for molten salt reactor licensing. Nucl. Eng. Des. **355**, 110308 (2019). https://doi.org/10.1016/j.nucengdes.2019.110308
46. G. Chiba, M. Tsuji, T. Narabayashi et al., Important fission product nuclides identification method for simplified burnup chain construction: Physor 2014. J. Nucl. Sci. Technol. **52**, 953–960 (2015). https://doi.org/10.1080/00223131.2015.1032381
47. P.K. Romano, N.E. Horelik, B.R. Herman, et al., Openmc: a state-of-the-art monte carlo code for research and development. Annals of Nuclear Energy **82**, 90–97 (2015). Joint International Conference on Supercomputing in Nuclear Applications and Monte Carlo 2013, SNA + MC 2013. Pluri- and Trans-disciplinarity, Towards New Modeling and Numerical Simulation Paradigms. https://doi.org/10.1016/j.anucene.2014.07.048
48. P.K. Romano, C.J. Josey, A.E. Johnson et al., Depletion capabilities in the openmc monte carlo particle transport code. Ann. Nucl. Energy **152**, 107989 (2021). https://doi.org/10.1016/j.anucene.2020.107989
49. M.L. Fensin, M.R. James, J.S. Hendricks et al., The new mcnp6 depletion capability. Proc. ICAPP **2012**, 24–28 (2012)
50. J. Leppänen, M. Pusa, T. Viitanen et al., The serpent monte carlo code: Status, development and applications in 2013. Ann. Nucl. Energy **82**, 142–150 (2015). https://doi.org/10.1016/j.anucene.2014.08.024
51. K. Wang, Z. Li, D. She et al., Rmc-a monte carlo code for reactor core analysis. Ann. Nucl. Energy **82**, 121–129 (2015). https://doi.org/10.1016/j.anucene.2014.08.048
52. G.G. Davidson, T.M. Pandya, S.R. Johnson et al., Nuclide depletion capabilities in the shift monte carlo code. Ann. Nucl. Energy **114**, 259–276 (2018). https://doi.org/10.1016/j.anucene.2017.11.042
53. T. Shannon, J. Wheeler, G. Touvannas, Tgbla/panacea and casmo/microburn analyses of ge9b/ge10 fuel in the quad cities. Trans. Am. Nuclear Soc. **74** (1996). https://www.osti.gov/biblio/436981
54. D. Knott, E. Wehlage, Description of the lancer02 lattice physics code for single-assembly and multibundle analysis. Nucl. Sci. Eng. **155**, 331–354 (2007). https://doi.org/10.13182/NSE155-331
55. H. Huria, R. Buechel, Recent improvements and new features in the westinghouse lattice physics codes. Trans. Am. Nuclear Soc. **72** (1995). https://www.osti.gov/biblio/186699
56. P. Archier, S. Domanico, J. Palau, et al., PHYSOR 2016-unifying theory and experiments in the 21st Century, validation of a multi-purpose depletion chain for burnup calculation through tripoli-4 calculations and ifp perturbation method (2016)
57. M.L. Fensin, M. Umbel, Testing actinide fission yield treatment in cinder90 for use in mcnp6 burnup calculations. Prog. Nucl. Energy **85**, 719–728 (2015). https://doi.org/10.1016/j.pnucene.2015.09.001
58. R.R. Yang, Y. Yuan, C. Hao et al., keff uncertainty quantification and analysis due to nuclear data during the full lifetime burnup calculation for a small-sized prismatic high temperature gas-cooled reactor. Nucl. Sci. Tech. **32**, 127 (2021). https://doi.org/10.1007/s41365-021-00969-w
59. A. Trkov, M. Herman, D. Brown, et al., Endf-6 formats manual. Brookhaven National Laboratory **80** (2012)
60. T.L. Schulz, Westinghouse ap1000 advanced passive plant. Nucl. Eng. Des. **236**, 1547–1557 (2006). https://doi.org/10.1016/j.nucengdes.2006.03.049
61. N. Stauff, T. Kim, T. Taiwo et al., Benchmark for neutronic analysis of sodium-cooled fast reactor cores with various fuel types and core sizes. Tech. Rep., Organisation for Economic Co-Operation and Development (2016)